Title: Local and global response of sandwich beams made of GFRP facings and PET foam core in three point bending test.

Authors: Łukasz Pyrzowski[a], Bartosz Sobczyk[a,*]

Affiliation:

[a] Gdansk University of Technology, Faculty of Civil and Environmental Engineering,

Department of Mechanics of Materials and Structures,

80-233 Gdańsk, Narutowicza 11/12, Poland

Abstract

In the paper behaviour of laminated sandwich beams (FRP face sheet – PET foam core – FRP face sheet) subjected to three point bending is studied. The paper aim is to find practical descriptions enabling effective and accurate estimation of the elastic response, damage and failure of the beams, basing on experiments and static calculations. Therefore a number of tests are described, that were done on laminated coupons and foam specimens in order to choose appropriate material models and find their constants. Experimental results of three-point bending tests of sandwich beams with three types of PET cores are analysed to evaluate the chosen material laws. The beam responses are predicted in numerical static simulations. The equations of problem are solved by means of finite element method (FEM). In the end the experimental and FEM results are compared. They are similar in terms of both their quantity and quality.

Keywords: Sandwich Structures; Glass Fibre Reinforced Plastics (GFRP); PET Foam Core; Crushable Foam Plasticity; Finite Element Method (FEM)

---

* Corresponding Author

e-mail address: bartosz.sobczyk@pg.edu.pl

1. Introduction and research background

Increasing interest in the use of modern hi-tech materials including different types of composites is observed nowadays. A lot of research is currently done in the field of evaluation of behaviour of the engineering structures built of the composites such as fibre reinforced plastics (FRP), fibre metal laminates (FML), functionally graded materials (FGM), sandwich structures or others, mainly by means of improved theoretical descriptions, experimental tests or sophisticated numerical calculations. Some selected recent achievements, considerations and studies in these fields are presented. One can find general papers that show examples of applications of composites [1–4]. Researchers deal with implementation of new theoretical descriptions enabling analyses of response or failure of composites [5–9]. Experimental and numerical studies of modern bridges and other structures made of composites are presented in [10–17]. Buckling and post-buckling response of engineering structures made of composites has also gathered interest [18–22]. In this paper the attention is focused on sandwich structures. The essential feature of a sandwich element, which is described in almost every paper dedicated to the analysis of structures of this type, is its high stiffness in bending accompanied by low weight. From this reason sandwich beams, shells, decks or plates are often used in various industries and to build engineering structures. Furthermore, because the structure concept is so attractive, there are numerous solutions including different types of cores or materials that are used to construct a sandwich. The number of possibilities in this field is still increasing, as the development of new materials and their application in engineering structures is very rapid and currently ongoing. In consequence, the behaviour of hi-tech sandwich composites has not been fully understood and the research in this area is still in high demand. Nevertheless, it has to be mentioned, that some approaches, allowing one to analyse response and behaviour of sandwich elements, have been already formulated. Papers describing experimentally measured behaviour are available (for example refer to [23–25]). What is more, organisations as e.g. American Society for Testing and Materials (ASTM) or International Organization for Standardization (ISO) have given recommendations in the field of material constants determination, enabling linear analysis of response and design of sandwich elements.

In this paper, we study nonlinear static global and local (including core failure) response of sandwich composites made of glass fibre reinforced plastic (GFRP) face sheets and PET foam cores, having different densities. Our intention is to show new experimental results, enabling better understanding of sandwich behaviour, especially beyond the linear response range. The main attention is

focused on computational analyses, aiming to recreate the observed behaviour. Recently published and interesting articles, related in a sense to the research done in this paper, are shortly discussed. In [26,27] experimental results of impact response of sandwich beams and panels are presented. Experimental studies of sandwich response under different static actions are shown in [13,25,28–31]. In [32] low velocity impact response is analysed and the resulting local failure of foam-based sandwich panels made of GFRP face sheets and PET or PVC foam core is considered. Numerical simulations aiming to recreate behaviour observed in experiments are presented. However, the constants of crushable foam plasticity model used by them to describe local foam failure are not provided in [32]. The paper [33] is also dedicated to experimental and numerical analyses of sandwich failure under dynamic impact. The sandwich specimens analysed in [33] are made of carbon fibre reinforced plastics (CFRP) and a PU foam, which damage is described via von Mises plasticity model. The paper [34] presents interesting experimental and numerical analyses of sandwich panels made of GFRP face sheets and PU foam, which are subjected to bending. Unfortunately, the constants of crushable foam plasticity material law are missing in [34], thus it is not possible to fully benefit from the presented results for example to analyse foam failure. There are also other, more sophisticated approaches that have been recently used in analyses of sandwich elements behaviour, as for instance [35,36]. Notwithstanding, because of their high scientific level, these models are either too complex to be used in solutions of engineering problems or are hardly accessible in finite element method (FEM) codes, therefore their wide applicability is rather contested.

Owing to the problems considered in the recently published papers, that are briefly described above, our intention is to present an approach to numerical modelling, justified by experimental observations, enabling appropriate description of global and local response of sandwich elements under static loads in both linear and nonlinear range, also including failure of foam core. This is very important regarding design of structures made of sandwich composites and further development and application of this promising structural solution, as a validated approach can give a very detailed insight into the response of a sandwich structure. Moreover, computational analyses can significantly facilitate the design process, as they are very useful in searching for an optimal solution. We search for an approach that can be easily and widely used by engineers and researchers, despite the fact that it is not standardized. In consequence, it requires the use of computational methods together with some sophisticated material laws, which also necessitate additional material properties identifications. Therefore, tests were performed on laminated GFRP coupons and PET foam specimens with three different densities: 80kg/m^3,

100 kg/m^3, 200 kg/m^3 in order to find material models that are suitable for the description of their response and to establish all the required constants. Main attention is focused on the PET foam, as its response can be strongly nonlinear and thus difficult to describe. In this case applicability of crushable foam plasticity material law is studied. This particular law seems to be suitable of capturing local deformations of foam under concentrated loads. The results of PET foam tests are compared with the available technical data sheets of the used materials to check appropriateness of shear modulus estimations. The chosen models are subsequently used in FEM calculations and validated against our results of three point bending experimental tests of sandwich beams. All the tests and calculations are described in detail and all the necessary data is included, allowing one to use the same models as presented here.

The study of recent literature revealed, that for sandwich structures built of particular set of materials, namely GFRP and PET foam such a computational analysis, preceded by numerous experiments, including especially identification of crushable foam plasticity material law constants, described and discussed in detail, has not been done yet. Therefore, our contribution enables development of knowledge in the use of composite materials in engineering structures, especially in the field of understanding of their behaviour and design of such elements. It is worth to mention, that the recommendations and conclusions presented in this paper have been already used by us in order to design and build a hi-tech sandwich footbridge [12,37].

2. Material properties testing

Before the essential research program (described in subsequent chapters) was developed and launched, some preliminary tests of sandwich beams response were done, in order to check what type of behaviour can be expected for the used materials and to prepare methods and devices suitable for the analyses. Therefore some three point bending tests of beams made of soft foam core, having different spans, were arranged and done until the moment of beams final failure, as shown in Fig. 1. The tests revealed that the FRP face sheets seem to remain undamaged and the failure of the whole beam is mainly caused by rapid shear failure of the core which is preceded by core crushing and followed by debonding of the face-core interface. Therefore, specific material models, capable of description of this behaviour are searched for here.

2.1.   FRP laminate

A ply of a laminated composite is commonly treated, when speaking about determination of its mechanical properties, as thin, homogenous, anisotropic, orthotropic or isotropic (depending on the type of the used reinforcement), although its microstructure is more complex. Such an approach, allows one to analyse response and behaviour of structures made of laminated composites in the solution of engineering or even more challenging scientific problems, see [8,18,19,38]. On the other hand some very detailed and sophisticated descriptions, in which for example the microstructure of the composite is modelled, are available [39,40]. These, however, are rarely used as compared to the previously described ones. Nevertheless, even when the ply is homogenized, the structural analysis is not so simple, because its response under different loading conditions can be generally nonlinear, as for example it is shown in [41] for the case of uniaxial tension tests and in [42] under pure shear conditions.

Due to this reasons some standards were formulated ([43–47]) that enable determination of elastic constants of homogenized ply of laminated composite built of unidirectional (UD), biaxial or multidirectional reinforcement. However, according to the standards, the elastic constants are calculated for a certain range of strains (ε or γ), which for example for the elastic modulus in tension in the fibre direction ranges from 0.05% to 0.25%. The standards neither comment the possible occurrence of nonlinearities in the response of the laminate, nor they recommend what to do in such a situation. Therefore, in fact, the recommendations are vague and unclear in this respect.

In this paper, laminated composites, made of biaxial, stitched and balanced BAT800 [0/90] or GBX800 [+/-45] E-glass fabrics and flame retardant vinylester resin, are analysed. Consequently, the composite ply will be denoted later on correspondingly as BAT or GBX, to emphasize that biaxial reinforcement is used. The elastic constants of the ply were identified according to [44,46,47], by the laboratory of Warsaw Military University of Technology, Poland (WMUT). They are described for instance in [48,49]. Basic identification tests on standard laminate coupons as uniaxial tension parallel to fibres in the fibre directions (refer to Fig. 2) and in-plane shear tests (see Fig. 3), have also been carried out by the research team from Gdańsk University of Technology (GUT). The constants identified at GUT are very similar to the ones determined by WMUT. The full set of elastic properties identified according to the standard procedures [43–47] is provided in Tab. 1 for the analysed homogenised ply with biaxial reinforcement, which average thickness is 0.663mm, in the temperature of 20°C. It is worth to mention that these properties are temperature dependent (refer to [37,48]). It has been found for the ply under

consideration that the stress-strain relations are nonlinear (refer to Fig. 2 and Fig. 3). The uniaxial tests of tension parallel to the reinforcement of BAT [0/90] only composites reveal that a decrease of stiffness of the material occurs approximately when the longitudinal strain ε equals 0.5%. This results from matrix microcracking and is known as the knee effect phenomenon (see also [50,51]).

The response of a quasi-isotropic composite during the uniaxial tension tests parallel to 0 direction fibres (refer to Fig. 4) has been also analysed at GUT. The considered composite comprise of 4 plies (total thickness of the composite is 2.65mm) and has the following sequence [BAT/GBX]$_s$, which formally is denoted as [0/90/+45/-45]$_s$. This test has been done to evaluate, whether the nonlinear shear affects its global response. Bi-linear stress-strain relation for the quasi-isotropic laminated composite has been obtained, similar to the one determined for the case of testing of composites made of BAT fabrics only (see Fig. 2) and with no signs of additional effects caused by shear nonlinearities. Therefore, for the quasi isotropic composite equivalent elastic properties can be determined. These are defined by tangent modulus, being 18.4GPa, when $ε \leq 0.5\%$ and 10.8GPa, when $ε > 0.5\%$. The Poisson's ratio determined in such a case in the experiment is roughly 0.3 in the whole range of strains under consideration.

The experimental tests, aiming to determine homogenized material properties of the lamina, described in this chapter allow us to state, that there are two ranges of its behaviour, namely before and after occurrence of matrix microcracking and that in case of in-plane shear the response is nonlinear. Therefore, when a detailed analysis of the laminate behaviour is done and large strains are observed in the plies the aforesaid effects should be included in the idealized model of the considered system. However, states characterised by small displacements and strains are considered when designing a structure. Therefore, it can be expected that the nonlinear effects resulting from matrix cracking or shear would not reveal in the lifetime of a structure. In consequence, in a case when the amount of strain occurring in ultimate limit state (ULS) is controlled and the response of the system is limited only to the linear undamaged range, it is fully justified to treat laminate properties as linear or quasi linear. This is in accordance with the procedures for the material properties determination available in the standards [43–47]. Such a design approach was used for instance in [12,37,38]. Hence, it can be stated that during the design it is assumed that undamaged material is used, which is beneficial regarding long-term operating conditions of a structure, as damage of load bearing layers can negatively affect the durability of the structure.

2.2.   PET foam

The appropriate choice of material model, being suitable for the description of stress-strain relation in a foam is important. However, there are various foams having extremely different properties, thus the task is not so simple and each type of foam needs to be carefully analysed. Usually, experimental identification of material properties of the foam is done. Procedures exist, according for example to ISO (e.g. [52–54]) or ASTM (e.g. [55–57]) standards, that enable determination of elastic and strength properties of the core, which are valid for PET foams as well. What is more, technical data sheets are provided for foams that are available on market, which include information on the most important material properties declared by producers and identified according to the aforesaid standards. In such a case it seems that the description of material behaviour should be easier. Nevertheless, the standards [52–57] give recommendations that can be helpful only when the elastic response of the core is considered. What is more, the fact that the foam can be generally anisotropic is not commented. From these reasons some difficulties can be encountered when detailed analyses of sandwich response are done and identification of the foam core materials properties according to standards seems to be insufficient in such a situation.

In this research, application of structural foam cores Armacell ArmaForm PET/W with three different densities 80, 100 and 200kg/m^3, which are denoted correspondingly as AC80, AC100 and AC200, has been considered. Each of the used foam cores has closed-cell structure. Their elastic properties and strengths, declared by the Producer and gathered in the technical data sheet [58] are given in Tab. 2. It is worth to mention, that the layout and type of information available in the technical data sheets (refer to Tab. 2) is common for many producers of structural foams. As it is shown in Tab. 2 the analysed PET foams have different elastic properties in tension and compression and only one shear modulus is provided. There is no information on Poisson's ratio in the data sheet, the material coordinate system of the core is neither included. The foams are generally treated as anisotropic materials. It needs to be emphasized that the foam sheets of sandwich cores are produced in a way that one dimension (thickness) is significantly smaller than the two remaining ones. For example for ArmaForm PET/W the sheets have the following dimensions 2448mm (length) × 1008mm (width) × 5-150mm (thickness). What is more the sandwich panels made of them are subjected to loads perpendicular to their plane. Hence, the material axes orientations are somehow tacitly assumed in the standard procedures of testing and typically the foam elastic moduli in-the-plane of the core and out-of-plane shear modulus are given. In the case of

basic calculations of bending response of sandwich beams or plates, the technical data is sufficient to describe the properties of materials, as for example analytical solutions require in-plane stiffness of laminate facings and out-of-plane shear modulus of sandwich core (refer to [59]), which is available in the technical data. Consequently, the problem of foam anisotropy can be omitted. However, when more complicated analysis is carried out, for instance by means of FEM, like in this paper, the core constitutive relation needs to be fully defined. To simplify the task, the foam core is often treated as an isotropic material, but the question arises: is it possible to efficiently and properly substitute anisotropic material for the isotropic one for every foam? In [32–34] isotropic material law is used to describe response of foam core of a sandwich element, but the Authors of these papers did not describe how the constants of isotropic continuum were determined or they do not give them at all.

In view of that the number of constants already described above seem to be not sufficient and more information needs to be collected. What is more, things are getting more complicated, when for instance nonlinear behaviour and failure of the foam core are studied, as it is done in this paper. In such a case advanced materials laws are used to describe nonlinear stress-strain relation in the foam. It has to be emphasized, that identification of their properties is beyond the scope of standard methods of material properties testing, e.g. [52–57].

In this paper, isotropic model with crushable foam plasticity with volumetric hardening (refer to [60]) is used to describe the response of the foam core. This particular one is chosen, as it is easy in use for engineers (isotropy) and because of the behaviour observed for the sandwich beams during the preliminary tests (plasticity). Additional descriptions enabling for example crack propagation analysis have not been employed. As the failure is very rapid, it will be possibly sufficient to find the onset of damage, which can be approximately treated as the moment of final failure. To describe the crushable foam plasticity law the following information needs to be gathered: elastic constants of isotropy, stress-strain relation for uniaxial compression, tensile and compression strengths and yield strengths in hydrostatic tension and compression. According to [60] the choice of tensile strength should not significantly affect the analysis results unless the foam is subjected to hydrostatic tension. As hydrostatic tension of the core is a rather rare state of loading, we are not going to identify tensile strengths in this paper. Uniaxial and hydrostatic compression tests are not included in standard recommendations for foam testing. This clearly shows, that in some situations non-standard testing needs to be employed to collect detailed data about properties of the core.

Appropriate experimental procedures have been selected to find the constants of the crushable foam constitutive relation, which are not however the ones that are chosen in a standard case. It is worth to mention here that it would be pointless to determine the elastic core properties basing on the data obtained in three point bending tests (for example according to [55]). This is because the appropriateness of the chosen material models (identified separately for facings and the core) is validated using the data gathered from three point bending tests. Such an approach should allow verification of correctness of all the identifications.

For each foam type, i.e. AC80, AC100 and AC200, the following tests have been conducted: three uniaxial compression tests in the core thickness direction (see Fig. 5, Fig. 6), done in accordance with guidelines [54] and three hydrostatic compression tests on cylindrical specimens (radius of each specimen equalled 50mm, height was 100mm), as presented in Fig. 7 and Fig. 8. The hydrostatic compression tests were done at the laboratory of the GUT Department of Geotechnics, Geology and Marine Civil Engineering. The results shown in Fig. 6 and Fig. 8 are presented as sample mean for each foam type. It has to be added, that the maximum hydrostatic pressure in the used testing apparatus is 1.2MPa, therefore it was not possible to find the yield strength in hydrostatic compression for the AC200 foam, as it turned out to be higher than this value (Fig. 8). Due to this reason it was estimated. Additional hydrostatic compression tests were done on AC150 foam to find its hydrostatic yield strength, which equalled 0.8MPa (see Fig. 8). It can be seen that (refer to Tab. 3 and Fig. 8) the hydrostatic compression strength is rising when the foam has higher density. The strength for AC150 ($f_c^{h,150}$) roughly equals twice the strength of AC100 ($f_c^{h,100}$) foam, while the strength of AC100 equals twice the strength of AC80 ($f_c^{h,80}$), so $f_c^{h,150}/ f_c^{h,100} = f_c^{h,100}/ f_c^{h,80} = \sim2$. In such a case it can be assumed that this relation holds also for AC200 strength ($f_c^{h,200}$), namely $f_c^{h,200}/ f_c^{h,150} = \sim2$. Thus, the hydrostatic compression strength of AC200 foam equals approximately 1.6MPa. This value is included in Tab. 3.

As a result of the experiments done on foam specimens, the following constants have been determined: elastic moduli in the foam thickness direction (according to [54]), uniaxial compression strengths (according to [54]) and yield strengths in hydrostatic compression, all of which are collected in Tab. 3. Therefore to fully define the isotropic relation either Poisson's ratio or shear modulus needs to be determined. It is also important that in the end, the law should enable description of global response of the element, which for the core is mainly dependent on the shear modulus, as well as local crushing of the core in the core thickness direction. From this reason, it can be stated that it is, in a sense, an equivalent

constitutive description, as particular behaviour is reflected by the law. It is observed, that for the analysed PET foams, the identified elastic moduli in the core thickness direction are lower than the values given by the producer in the technical data (Tab. 2), which confirms that the analysed foam is anisotropic. The recommendations of DIAB company ([61]), other distributor of structural foam cores, indicate that overestimated values of Poisson's ratio will be obtained, due to un-isotropic cell structure of foam, when it is calculated from the elastic and shear moduli given in technical data sheet (refer to Tab. 2). As the elastic moduli identified and shown in this paper are lower than the ones provided by the producer, it seems that it can be used to find the aforesaid equivalent law. From this reason an attempt was made to experimentally determine the foam Poisson's ratio. Unfortunately, the results were strongly scattered, making it unable to draw any conclusions about the ratio. No results of experimentally identified Poisson's ratio have been found in the literature as well. Nevertheless, Phoenix Technologies International, LLC, manufacturer of recycled PET (the same material is used to produce the Armacell ArmaForm PET/W core), reports that the Poisson's ratio for PET ranges from 0.37 to 0.44, depending on the deformations direction. Therefore, it is assumed that the Poisson's ratio for all the PET foams considered in this paper is 0.4. In consequence the resulting shear moduli, calculated for AC80, AC100 and AC200 on its basis and using the identified elastic moduli in the core thickness direction, are given in Tab. 4. These are compared with the ones reported by the core producer, which were identified using the standard [53], in Tab. 4 as well. The difference between them ranges from 1.5% to 5.8% depending upon the foam type and thus is very small.

Therefore, we can say that we did manage to find equivalent technical constants of isotropic material law for the considered PET foams, which on the one hand enable to assign appropriate shear stiffness to the core via the shear modulus, and on the other hand enable description of local failure as a consequence of crushing, during which the elastic modulus in the foam thickness direction is important.

In Tab. 5 the experimentally identified parameters of crushable foam material law are collected. These can be used as analysis input data. In Fig. 9, the curves defining volumetric hardening of the constitutive relations are presented, which were created after simplifications and data processing of experimental uniaxial compression results (Fig. 6), because the hardening needs to be given in ascending magnitude of the plastic strain ([60]). It has to be emphasized that the default value (according to [60]) of hydrostatic yield stress ratio is given in Tab. 5, because yield strength in hydrostatic tension has not been

identified. This is because the choice of tensile strength should not significantly affect the numerical results unless the foam is subjected to hydrostatic tension ([60]), which is not the case here.

3. Three point bending tests

3.1. *Experiments*

Three point bending tests (3p tests) have been conducted in order to measure the real response of composite sandwich beams, which were made of the materials described in detail in chapters 2.1 and 2.2, namely FRP face sheets (BAT [0/90] or GBX[+/-45] fabrics and vinylester resin) and PET foams having different densities. At this point, it is worth to mention the reason that AC80, AC100 and AC200 cores have been considered. The other aim of this research was to find a core that can be used to design and construct a hi-tech sandwich composite footbridge (see [12,37]), thus different foams had been analysed to find the appropriate one. The beams face sheets were the same for all the beams and each had the ply sequence [BAT/GBX]$_s$, or using formal denotation [0/90/+45/-45]$_s$. The 1st material axis (0 direction of reinforcement) was parallel to the beam longitudinal axis. Two beams were manufactured from each type of structural core. Therefore, six beams were manufactured in total. The beams were created in the following way. At first sandwich plates were manufactured using vacuum infusion process. Then the plates were appropriately cut into pieces and the beams were produced, all of which had the same dimensions, i.e., they were 1220mm long, 90mm wide and 75mm high (core thickness). They were put on the test stand presented in Fig. 10, in a way that is shown in Fig. 11, thus the span length of each beam in 3p test was 1000mm. The cross-head and supports were solid half–cylinders (cylinder radius equals 40mm), made of steel. Zwick/Roell Z400 testing machine was used to do the tests. The speed of the cross–head in all the tests was 4mm/min. The following devices were used to gather data about the responses of the beams: Zwick/Roell software to save the total force applied to each beam and the displacement of cross-head; displacement inductive sensor to measure vertical displacement of the lower FRP face sheets at the beam mid-span; three strain gauges, denoted as T1, T2 and T3, as shown in Fig. 10, to measure strain of FRP face sheets in different locations. Pictures of the beams were also taken during the tests in order to capture and document their deformation and failure modes. All the experiments were carried out up to the moment of beams failure. During the experiments, the beams failure was investigated without using any advanced methods, as for example acoustic emission [62,63]. This was due to the fact that the beams during the preliminary tests failed suddenly. The failure was not

preceded by the following effects that could have been observed visually: openings or excessive slippage at the core-face sheets interface, cracks of the face sheets or cracks of the foam core. Moreover, no acoustic effects, that could have been heard, occurred before final failure during the tests. Nevertheless, observations of changes in the values of force that was applied to the beams by the testing machine (using displacement control technique) were done. If the force drops before final failure, this means that the structure received some damage. The choice of such a rough, simplified approach to determining damages of the sandwich beams was justified by the fact that the main attention was focused on their final failure, which was very rapid and therefore it was not necessary to use advanced sensors to capture it. Nevertheless, this has been additionally verified in numerical analyses, which are described in the next chapters.

3.2.   *Numerical calculations*

Numerical models of each type of beam were built and 3p tests were simulated by means of nonlinear static calculations, including material nonlinearities and effects of large deformations and displacements, in order to verify if the material models, discussed and chosen for FRP face sheets and PET foams in chapters 2.1 and 2.2 are appropriate for the description of the sandwich behaviour. The equations of the problem have been solved using FEM.

The computational models were created in Abaqus 6.14 software. The face sheets are built of 4-node general purpose, structural shell elements with linear shape functions, reduced integration and hourglass control, denoted as S4R. Whereas, 8-node linear, brick, continuum elements with reduced integration and hourglass control, labelled as C3D8R, were used to build the core. No spurious zero energy modes were observed in our calculations, that could have affected the solution, although finite elements with reduced integration were used for the purpose of description of deformable parts of the beams. The steel supports and the steel cross-head were modelled using 4-node, bilinear quadrilateral rigid elements, denoted as R3D4, because their deformations were negligible during the tests and such an approach reduced the numerical effort required to get the solution. What is more, only a quarter of each beam was modelled and appropriate symmetry conditions were assigned. This is because of the symmetry of the beams geometry, boundary and loading conditions and material properties of the system. In consequence the size of the task was significantly reduced. Such a treatment of the problem is valid to the moment of failure initiation of the beam and this is the range of interest in this paper. The smallest size of

finite element edge in the model was 2.5mm, while the biggest one was 6mm long. The mesh was refined in the zones where local influences are important, namely in the vicinity of cross-head and above the supports. It was coarsened in other regions. The aspect ratio of finite elements ranged between 1 and 2. The computational model contained 49666 nodes and 44055 elements in total and its visualisation is shown in Fig. 12. The used mesh of finite elements is very fine and underwent mesh convergence study.

Appropriate constants of isotropic model with crushable foam plasticity and volumetric hardening were assigned to the core depending on the considered foam type. They are gathered in Tab. 5 and Fig. 9. The FRP face sheets in the analysis of beams with AC80 and AC100 cores were treated as elastic orthotropic in plane stress, due to the amount of strain, which did not exceed 0.5% (refer to chapter 2.1 and Fig. 4). Therefore each, appropriately orientated ply (0.663mm thick) of the face sheets, was endowed with the properties from Tab. 1. The strains in the laminate face sheets for the beams with AC200 core were greater than 0.5%. Thus in this case, the whole face sheets (being 2.65mm thick) were treated as isotropic and bilinear stress–strain relation with constant values of tangent moduli, being 18.4GPa, when $\varepsilon \leq 0.5\%$ and 10.8GPa, when $\varepsilon > 0.5\%$, were assigned to them. The Poisson's ratio was 0.3.

The face sheets were perfectly bonded to the core in the analysis, as no symptoms of debonding between them and the core prior final failure, as for example openings, excessive slippage at the interface, or decrease of the force, controlled by the displacement of the testing machine cross-head and applied to the beam, were observed. A contact formulation was used to describe interaction between cross-head and upper face sheet and between steel support and lower FRP facing. The contact description included normal behaviour ("hard" contact with allowance of separation after contact) and tangential behaviour (penalty formulation with friction coefficient that equals 0.297). The following boundary conditions were applied to the model: steel supports were fixed, symmetry conditions were applied on the appropriate planes of the beam quarter, cross-head was fixed with exception of its vertical translation. A certain value of vertical displacement was assigned to the cross-head to simulate its movement during the static analysis. The Newton's method was the numerical technique used for solving nonlinear equilibrium equations ([60]).

According to our observations during preliminary and final 3p tests, the core failed rapidly because of shear (beams with soft foam cores) or the beams were destructed when upper face sheets suddenly debonds from the core (AC200 core). No signs of failure of the face sheets were found in all the tests. It is

claimed that the sudden failure of the core or the debonding at the face–core interface is due to the insufficient shear resistance of the core or a particular state of stress appearing at the interface that equals the bonding strength. In such a case when a damage is initiated it propagates very rapidly. Therefore, all the FEM calculations were terminated when either maximum shear stress in the foam reached the core shear strength or the stresses at the interface reached bonding strength. This moment was treated as the failure load of the sandwich beam.

3.3.   Results and discussion

The character of deformation as well as the failure mode of the beams made of AC80 and AC100 cores are different than for beams with AC200 core. Vertical displacements of the sandwiches built of AC80 and AC100 cores change linearly along the beams and the lines of beams deflections are some piecewise linear curves made of two segments. This is because of low shear stiffness of the used cores. During the experiments we observed that the beam responses were linear at first, then at a certain moment plastic crushing of the foam was initiated. Finally, a major shear crack propagated rapidly through the core, resulting in the beam failure. The deformations shortly before failure and the failure modes of the AC80 and AC100 beams are shown in Fig. 13- Fig. 16. The stiffness of the AC200 core is much greater than in previous cases. In consequence, the beam deflection line is parabolic (refer to Fig. 17). The range of the AC200 beams linear response is significantly larger than for the beams with softer cores. The plastic deformation is noticeably smaller than for the AC80 and AC100 beams, is initiated shortly before AC200 beam failure, which occurs because the upper face sheet debonds suddenly from the core, as shown in Fig. 18. In Fig. 13-Fig. 18 the corresponding FEM estimations of beam deformations and contours of the maximum shear stress, that are used to explain the beams failure mechanisms, are also shown. The aforesaid deformations of beams seem to be well predicted by means of FEM calculations and will be further analysed using precisely measured values in the next chapters. The discussion about the final failure will be done later as well. It is worth noting, that in Fig. 13- Fig. 18 some visualisation of FEM results on beams without symmetry, are presented, although models of beam quarters were only done. This eases the process of experimental vs. FEM beam deformations analysis and comparisons.

By using the network of sensors (described in 3.1) a lot of data about the beams responses was gathered that can be examined and is useful in understanding of sandwich behaviour and evaluation of the modelling approaches done in this paper. Therefore experimentally registered values and the

corresponding FEM estimations of the following relations can be analysed: cross-head force vs. cross-head displacement; cross-head force vs. reduction of the core thickness at the mid-span (Δh); cross-head force vs. longitudinal strain in FRP face sheets at T1, T2 and T3 locations. These are shown for all the analysed beams in Fig. 19 – Fig. 27. It is worth to mention that the reduction of the core thickness was calculated as vertical displacement of the lower FRP face sheet at the beam mid-span (taken from displacement inductive sensor) subtracted from cross-head displacement.

If the difference between P1 and P11 results, obtained for each type of the core in experiments only (see Fig. 19 – Fig. 27), is studied, it can be said that scattering of values is the greatest for the AC80 core in the case of T1 and T3 strain measurements (Fig. 21). Thus, these results are treated as inaccurate. It was observed that the lower face sheets of the beams made of AC80 foam were not precisely flat and parallel to the upper face sheets and it took time for these beams to adjust to the test stand during the experiments. This in conjunction with small stiffness of the core could have resulted in a low accuracy of results in the supporting zones. The remaining experimentally measured values for the AC80 beams, as well as all of them for elements made of AC100 and AC200 foams are quite repeatable and therefore accepted as accurate.

In consequence the differences between the measured values (obtained from the used sensors and devices) and FEM responses can be studied and thus it can be justified whether the numerical models reflect the observed behaviour of the sandwich beams. If the T1 and T3 strain results for AC80 specimens are now neglected, from the aforementioned reasons, it is claimed that the accuracy of the numerical estimations, considered here, is very good. This applies to the parameters reflecting global beams responses at the mid–spans, namely displacements (Fig. 19, Fig. 22, Fig. 25) and T2 strains (Fig. 21, Fig. 24, Fig. 27), as well as to the T1 and T3 strains (Fig. 24, Fig. 27), which are registered close to the supports. It is worth also to mention, that the estimated by means of FEM linear range of beams response, so important in the design of such elements is very similar to the experimental one.

The comparison between experimental and FEM failure mechanisms and loads of sandwich beams is presented in Tab. 6 Fig. 14, Fig. 16 and Fig. 18. In Tab. 6 P^{avg} stands for arithmetical mean of experimental failure loads of P1 and P11 specimens. The attention is now focused at the moment when the maximum shear stress reaches the core shear strength in the FEM analysis in the first element in the vicinity of the cross–head. The stress distributions in the AC80 or AC100 cores (Fig. 14 and Fig. 16) reveal an inclined band of the maximum shear stresses running from the top to the bottom face sheet. The

values of stresses within the bands are high and very close to the shear strength in the upper part of the core and approximately only 30% lower at the core–bottom face sheet interface. This explains why a major shear crack starting right under the cross-head sides is propagating through the core to reach the lower face sheet. On the other hand, if the maximum shear stress distributions are considered for AC200 beams, similarly as it has been done for AC80 and AC100 ones, it is seen (Fig. 18) that now the band of maximum shear stress is not formed. Instead, it is visible that the maximum shear stresses equal the shear strength of the AC200 foam at the core–upper face sheet interface under the cross head. The values of maximum shear stress near the bottom face sheet are less than 50% of the core shear strength. This explains why a major shear crack is not formed. During calculations also the state of stress at the interface was monitored. When the stresses at the interface equal its bonding strength, the interface fails. The bonding strength of the interface between the facings and the core, analysed in this paper, depends on the strength of the weakest material. This was confirmed by visual inspection of the failed AC200 beams. Therefore, it depends on the foam strength properties. The tensile stresses normal to the interface are well below the corresponding foam strength. However, the maximum shear stresses at the interface, in the vicinity of the cross-head, equal the foam shear strength. What is more these stresses appear and act on a plane parallel to the facings. From this reason it is claimed that this particular state of shear stresses that dominates at the interface causes the damage. Hence, forward shear bond failure is observed, which in fracture mechanics is denoted as mode II debonding [59].

The values collected in Tab. 6 show that for AC80 and AC100 beams the numerical estimations of final failure loads are very close to the experimental ones (relative difference between them ranges from 3.4% to 3.7%). The local crushing of foam, expressed by the Δh parameter is also predicted well for these cores (Fig. 20, Fig. 23). The FEM prediction of failure load of AC200 beam is slightly underestimated, it is 10.3% lower than the reference one. It was observed during infusion manufacturing of the beams that more resin was used than it had been planned to produce them. Thus, in our opinion, the foam at the interface with the face sheets could have absorbed more resin and hence a layer near the core–face interface has properties which are better than the ones identified for the pure foam that are included in the computational model. Due to this reason, the load initiating failure of the beam at the interface in the experiments is possibly slightly higher compared to FEM predictions. It is visible also in Fig. 26 that the numerical estimation of the Δh parameter is underestimated as compared to the experimental values. Also some differences between P1/AC200 and P11/AC200 experimental responses are observed. The

ArmaForm structural foams have small holes, running in the core thickness direction. The holes are arranged in a rectangular array. The distance between the holes in both orthogonal directions is the same and equals 60mm. These holes enable resin flow between top and bottom face sheets during the vacuum infusion process. Thus, additional columns having small diameter and height, the same as core height, are formed during manufacturing. These columns can affect the obtained results, especially the Δh parameter, when they are located exactly under the cross-head. During the manufacturing the location of columns in relation to the cross-head position was not set in any manner. Some of the beams had columns exactly under the cross-head, while other did not. Moreover, in some beams one row of columns was created, whereas in others, two rows were formed. This is shown in Fig. 28. This may be the reason that differences between the Δh parameter are observed for P1/AC200 and P11/AC200 experimental responses. The additional columns were neglected in numerical analyses. This can be the reason of underestimation of the FEM Δh values visible in Fig. 26. What is more the uniaxial compression tests of AC200 beams revealed that, the material response exhibit slight weakening, right after the compression strength is achieved (Fig. 6). This effect cannot be taken into account in the crushable foam model, because the hardening needs to be given in ascending magnitude of the plastic strain, as it is presented in (Fig. 9). In consequence, the compression strength of AC200 foam is in the computational model approximately 10% lower than the strength of the real material, which could result in underestimation of the force–cross head displacement (Fig. 25) and force – Δh parameter FEM results (Fig. 26).

Concluding, the numerically obtained results are satisfying in terms of both quality and quantity. The global and local response of the face sheets and the core can be predicted with good accuracy. Therefore, the key properties of the sandwich beams seem to be appropriately chosen in view of the presented results. Hence, the approaches to modelling of the used materials, especially for the foam, which is treated, as isotropic (although it is orthotropic) with elastic constants derived to reflect out–of plane shear modulus of the core sheet and elastic modulus in the direction of its thickness, are justified.

4. Final remarks

In this paper local and global responses of sandwich beams made of GFRP face sheets and PET foam cores in three point bending tests were studied. Considerations leading to the choice of material models that can be successfully used in the analysis of sandwich beams behaviour were presented. This also included identification of material parameters, that was done experimentally on coupons made from GFRPs and different foam specimens. It was found that for laminate face sheets a control of strains needs

to be done in order to check whether microcracking of matrix is initiated which results in decrease of the laminate stiffness. The description of foam material model is more complicated, as the core can experience irreversible deformation. From this reason the isotropic crushable foam model with volumetric hardening was used for the core. An attempt was made to find isotropic constants describing foam behaviour, although, the foam is generally anisotropic. It turned out, that it is possible to determine material properties that enable appropriate description of global response of the core due to shear and also reflect the stiffness of foam when local crushing occurs. Analysis of maximum shear stress distributions in the core and the state of stresses at the facing-core interface allowed to draw conclusions about the reasons of beams failure, which was rapid due to shear (AC80 and AC100 cores) or upper face sheet debonding (AC200 core). In effect, it was possible to estimate the behaviour of the analysed sandwich beams by means of FEM with very good accuracy at global and local level. All the analysed numerical results, including also predictions of linear range of the beams response, being of crucial importance during the design of sandwich elements, were very close to the corresponding experimental ones. The experimental results were collected by a network of sensors giving a detailed insight into the beams responses. The material models chosen and the numerical models built for the purpose of analyses presented in this paper are relatively simple and available to other researchers. What is more the parameters of the constitutive relations of the materials used here are given, thus they are ready for application by other researchers for example to design similar elements. The conclusions from this research have been additionally checked during the tests of a 3 m long bridge segment subjected to different loading conditions [11]. A footbridge was manufactured from the same materials and tested. The measurements of its static and modal properties [12,37] confirmed that the behaviour of sandwich made of GFRP face sheets and PET foam is now understood and properly described thanks to the results described and discussed here.

Data availability

The raw/processed data required to reproduce these findings cannot be shared at this time due to technical or time limitations.

References

[1] Al-saadi AU, Aravinthan T, Lokuge W. Structural applications of fibre reinforced polymer (FRP) composite tubes: A review of columns members. Compos Struct 2018;204:513–24. doi:10.1016/j.compstruct.2018.07.109.

[2] Kabir SMF, Mathur K, Seyam A-FM. A critical review on 3D printed continuous fiber-reinforced composites: History, mechanism, materials and properties. Compos Struct 2020;232:111476. doi:10.1016/j.compstruct.2019.111476.

[3] Kim YJ. State of the practice of FRP composites in highway bridges. Eng Struct 2019;179:1–8. doi:10.1016/j.engstruct.2018.10.067.

[4] Parghi A, Alam MS. A review on the application of sprayed-FRP composites for strengthening of concrete and masonry structures in the construction sector. Compos Struct 2018;187:518–34. doi:10.1016/j.compstruct.2017.11.085.

[5] Burzyński S, Chróścielewski J, Daszkiewicz K, Witkowski W. Geometrically nonlinear FEM analysis of FGM shells based on neutral physical surface approach in 6-parameter shell theory. Compos Part B Eng 2016;107:203–13. doi:10.1016/j.compositesb.2016.09.015.

[6] Moleiro F, Carrera E, Ferreira AJM, Reddy JN. Hygro-thermo-mechanical modelling and analysis of multilayered plates with embedded functionally graded material layers. Compos Struct 2019:111442. doi:10.1016/j.compstruct.2019.111442.

[7] Nguyen LB, Nguyen N V., Thai CH, Ferreira AMJ, Nguyen-Xuan H. An isogeometric Bézier finite element analysis for piezoelectric FG porous plates reinforced by graphene platelets. Compos Struct 2019;214:227–45. doi:10.1016/j.compstruct.2019.01.077.

[8] Sabik A. Progressive failure analysis of laminates in the framework of 6-field non-linear shell theory. Compos Struct 2018;200:195–203. doi:10.1016/j.compstruct.2018.05.069.

[9] Sofiyev AH. The stability analysis of shear deformable FGM sandwich conical shells under the axial load. Compos Struct 2017;176:803–11. doi:10.1016/j.compstruct.2017.06.022.

[10] Arslan K, Gunes R. Experimental damage evaluation of honeycomb sandwich structures with Al/B4C FGM face plates under high velocity impact loads. Compos Struct 2018;202:304–12. doi:10.1016/j.compstruct.2018.01.087.

[11] Chróścielewski J, Ferenc T, Mikulski T, Miśkiewicz M, Pyrzowski Ł. Numerical modeling and experimental validation of full-scale segment to support design of novel GFRP footbridge. Compos Struct 2019;213:299–307. doi:10.1016/j.compstruct.2019.01.089.

[12] Chróścielewski J, Miśkiewicz M, Pyrzowski Ł, Rucka M, Sobczyk B, Wilde K. Modal properties identification of a novel sandwich footbridge – Comparison of measured dynamic response and FEA. Compos Part B Eng 2018;151:245–55. doi:10.1016/j.compositesb.2018.06.016.

[13] Kulpa M, Siwowski T. Stiffness and strength evaluation of a novel FRP sandwich panel for bridge redecking. Compos Part B Eng 2019;167:207–20. doi:10.1016/j.compositesb.2018.12.004.

[14] Mazurkiewicz Ł, Małachowski J, Damaziak K, Tomaszewski M. Evaluation of the response of fibre reinforced composite repair of steel pipeline subjected to puncture from excavator tooth. Compos Struct 2018;202:1126–35. doi:10.1016/j.compstruct.2018.05.065.

[15] Siwowski T, Kulpa M, Rajchel M, Poneta P. Design, manufacturing and structural testing of all-

composite FRP bridge girder. Compos Struct 2018;206:814–27. doi:10.1016/j.compstruct.2018.08.048.

[16]   Tuwair H, Drury J, Volz J. Testing and evaluation of full scale fiber-reinforced polymer bridge deck panels incorporating a polyurethane foam core. Eng Struct 2019;184:205–16. doi:10.1016/j.engstruct.2019.01.104.

[17]   Zhang D, Zhao Q, Li F, Tao J, Gao Y. Torsional behavior of a hybrid FRP-aluminum space truss bridge: Experimental and numerical study. Eng Struct 2018;157:132–43. doi:10.1016/j.engstruct.2017.12.013.

[18]   Debski H, Rozylo P, Gliszczynski A, Kubiak T. Numerical models for buckling, postbuckling and failure analysis of pre-damaged thin-walled composite struts subjected to uniform compression. Thin-Walled Struct 2019;139:53–65. doi:10.1016/j.tws.2019.02.030.

[19]   Debski H, Teter A. Effect of load eccentricity on the buckling and post-buckling states of short laminated Z-columns. Compos Struct 2019;210:134–44. doi:10.1016/j.compstruct.2018.11.044.

[20]   Kamocka M, Mania RJ. Post-buckling response of FML column with delamination. Compos Struct 2019;230:111511. doi:10.1016/j.compstruct.2019.111511.

[21]   Mao J-J, Zhang W. Buckling and post-buckling analyses of functionally graded graphene reinforced piezoelectric plate subjected to electric potential and axial forces. Compos Struct 2019;216:392–405. doi:10.1016/j.compstruct.2019.02.095.

[22]   Kolanu NR, Raju G, Ramji M. Experimental and numerical studies on the buckling and post-buckling behavior of single blade-stiffened CFRP panels. Compos Struct 2018;196:135–54. doi:10.1016/j.compstruct.2018.05.015.

[23]   Xanthos M, Dhavalikar R, Tan V, Dey SK, Yilmazer U. Properties and Applications of Sandwich Panels Based on PET Foams. J Reinf Plast Compos 2001;20:786–93. doi:10.1177/073168401772678562.

[24]   Fathi A, Keller J-H, Altstaedt V. Full-field shear analyses of sandwich core materials using Digital Image Correlation (DIC). Compos Part B Eng 2015;70:156–66. doi:10.1016/j.compositesb.2014.10.045.

[25]   Manalo A, Surendar S, van Erp G, Benmokrane B. Flexural behavior of an FRP sandwich system with glass-fiber skins and a phenolic core at elevated in-service temperature. Compos Struct 2016;152:96–105. doi:10.1016/j.compstruct.2016.05.028.

[26]   Caliskan U, Apalak MK. Low velocity bending impact behavior of foam core sandwich beams: Experimental. Compos Part B Eng 2017;112:158–75. doi:10.1016/j.compositesb.2016.12.038.

[27]   Akil Hazizan M, Cantwell WJ. The low velocity impact response of foam-based sandwich structures. Compos Part B Eng 2002;33:193–204. doi:10.1016/S1359-8368(02)00009-4.

[28]   Mathieson H, Fam A. High cycle fatigue under reversed bending of sandwich panels with GFRP skins and polyurethane foam core. Compos Struct 2014;113:31–9. doi:10.1016/j.compstruct.2014.02.027.

[29]   Iyer SV, Chatterjee R, Ramya M, Suresh E, Padmanabhan K. A Comparative Study Of The Three Point And Four Point Bending Behaviour Of Rigid Foam Core Glass/Epoxy Face Sheet Sandwich Composites. Mater Today Proc 2018;5:12083–90. doi:10.1016/j.matpr.2018.02.184.

[30]   Garrido M, Correia JR, Keller T. Effects of elevated temperature on the shear response of PET and PUR foams used in composite sandwich panels. Constr Build Mater 2015;76:150–7. doi:10.1016/j.conbuildmat.2014.11.053.

[31]   CoDyre L, Fam A. The effect of foam core density at various slenderness ratios on axial strength of sandwich panels with glass-FRP skins. Compos Part B Eng 2016;106:129–38. doi:10.1016/j.compositesb.2016.09.016.

[32]   Zhou J, Hassan MZ, Guan Z, Cantwell WJ. The low velocity impact response of foam-based sandwich panels. Compos Sci Technol 2012;72:1781–90. doi:10.1016/j.compscitech.2012.07.006.

[33]   Long S, Yao X, Wang H, Zhang X. Failure analysis and modeling of foam sandwich laminates under impact loading. Compos Struct 2018;197:10–20. doi:10.1016/j.compstruct.2018.05.041.

[34]   Tuwair H, Hopkins M, Volz J, ElGawady MA, Mohamed M, Chandrashekhara K, et al. Evaluation of sandwich panels with various polyurethane foam-cores and ribs. Compos Part B Eng 2015;79:262–76. doi:10.1016/j.compositesb.2015.04.023.

[35]   Arruda MRT, Garrido M, Castro LM., Ferreira AJM, Correia JR. Numerical modelling of the creep behaviour of GFRP sandwich panels using the Carrera Unified Formulation and Composite Creep Modelling. Compos Struct 2018;183:103–13. doi:10.1016/j.compstruct.2017.01.074.

[36]   Gebhart TMJ, Jehnichen D, Koschichow R, Müller M, Göbel M, Geske V, et al. Multi-scale modelling approach to homogenise the mechanical properties of polymeric closed-cell bead foams. Int J Eng Sci 2019;145:103168. doi:10.1016/j.ijengsci.2019.103168.

[37]   Chróścielewski J, Miśkiewicz M, Pyrzowski Ł, Sobczyk B, Wilde K. A novel sandwich footbridge - Practical application of laminated composites in bridge design and in situ measurements of static response. Compos Part B Eng 2017;126:153–61. doi:10.1016/j.compositesb.2017.06.009.

[38]   Siwowski T, Rajchel M, Kaleta D, Własak L. The First Polish Road Bridge Made of FRP Composites. Struct Eng Int 2017;27:308–14. doi:10.2749/101686617X14881932436339.

[39]   Obert E, Daghia F, Ladevèze P, Ballere L. Micro and meso modeling of woven composites: Transverse cracking kinetics and homogenization. Compos Struct 2014;117:212–21. doi:10.1016/j.compstruct.2014.06.035.

[40]   Abu-Farsakh GAF, Al-Jarrah HM. Micro-mechanical damage model accounting for composite material nonlinearity due to matrix-cracking of unidirectional composite laminates. Compos Sci Technol 2018;167:268–76. doi:10.1016/j.compscitech.2018.08.012.

[41]   Reis EM, Rizkalla SH. Material characteristics of 3-D FRP sandwich panels. Constr Build Mater 2008;22:1009–18. doi:10.1016/j.conbuildmat.2007.03.023.

[42]   Sabik A. Direct shear stress vs strain relation for fiber reinforced composites. Compos Part B Eng 2018;139:24–30. doi:10.1016/j.compositesb.2017.11.057.

[43]   ISO 527-1:2019 Plastics - Determination of tensile properties - Part 1: General principles, n.d.

[44]   ISO 527-4:1997 Plastics - Determination of tensile properties - Part 4: Test conditions for isotropic and orthotropic fibre-reinforced plastic composites, n.d.

[45]   ISO 527-5:2009 Plastics - Determination of tensile properties - Part 5: Test conditions for unidirectional fibre-reinforced plastic composites, n.d.

[46]   ISO 14129:1997 Fibre-reinforced plastic composites - Determination of the in-plane shear

stress/shear strain response, including the in-plane shear modulus and strength, by the plus or minus 45 degree tension test method, n.d.

[47]   ISO 14126:1999 Fibre-reinforced plastic composites — Determination of compressive properties in the in-plane direction, n.d.

[48]   Klasztorny M, Nycz DB, Romanowski RK, Gotowicki P, Kiczko A, Rudnik D. Effects of Operating Temperatures and Accelerated Environmental Ageing on the Mechanical Properties of a Glass-Vinylester Composite. Mech Compos Mater 2017;53:335–50. doi:10.1007/s11029-017-9665-9.

[49]   Chróścielewski J, Klasztorny M, Nycz D, Sobczyk B. Load capacity and serviceability conditions for footbridges made of fibre-reinforced polymer laminates. Roads Bridg - Drog i Most 2014;13:189–202. doi:10.7409/rabdim.014.013.

[50]   Yang B, Kozey V, Adanur S, Kumar S. Bending, compression, and shear behavior of woven glass fiber–epoxy composites. Compos Part B Eng 2000;31:715–21. doi:10.1016/S1359-8368(99)00052-9.

[51]   Wen C, Yazdani S. Anisotropic damage model for woven fabric composites during tension–tension fatigue. Compos Struct 2008;82:127–31. doi:10.1016/j.compstruct.2007.01.003.

[52]   ISO 1926:2005 Rigid cellular plastics - Determination of tensile properties, n.d.

[53]   ISO 1922:2018 Rigid cellular plastics - Determination of shear properties, n.d.

[54]   ISO 844:2014 Rigid cellular plastics - Determination of compression properties, n.d.

[55]   ASTM C273 / C273M - 19 Standard Test Method for Shear Properties of Sandwich Core Materials, n.d.

[56]   ASTM C297 / C297M - 16 Standard Test Method for Flatwise Tensile Strength of Sandwich Constructions, n.d.

[57]   ASTM C365 / C365M - 16 Standard Test Method for Flatwise Compressive Properties of Sandwich Cores, n.d.

[58]   ArmaForm   PET/W   AC: structural   foam   core   technical   data   2014. http://armacell.si/C1256AF100412A28/F/NT0041324A/$FILE/AC_W_EU.pdf.

[59]   Carlsson LA, Kardomateas GA. Structural and Failure Mechanics of Sandwich Composites. vol. 121. Dordrecht: Springer Netherlands; 2011. doi:10.1007/978-1-4020-3225-7.

[60]   Abaqus 6.14 Documentation, n.d.

[61]   DIAB guide to core and sandwich 2012:1–48. https://www.diabgroup.com/~/media/Files/Manuals-Guides/Diab Guideline to Core and Sandwich.pdf.

[62]   Tabrizi IE, Kefal A, Zanjani JSM, Akalin C, Yildiz M. Experimental and numerical investigation on fracture behavior of glass/carbon fiber hybrid composites using acoustic emission method and refined zigzag theory. Compos Struct 2019;223:110971. doi:10.1016/j.compstruct.2019.110971.

[63]   Kubiak T, Samborski S, Teter A. Experimental investigation of failure process in compressed channel-section GFRP laminate columns assisted with the acoustic emission method. Compos Struct 2015;133:921–9. doi:10.1016/j.compstruct.2015.08.023.

Figures

(a)

(b)

Fig. 1 Preliminary three point bending tests: long (a) and short (b) beams at the moment of failure

(a)

(b)

(c)
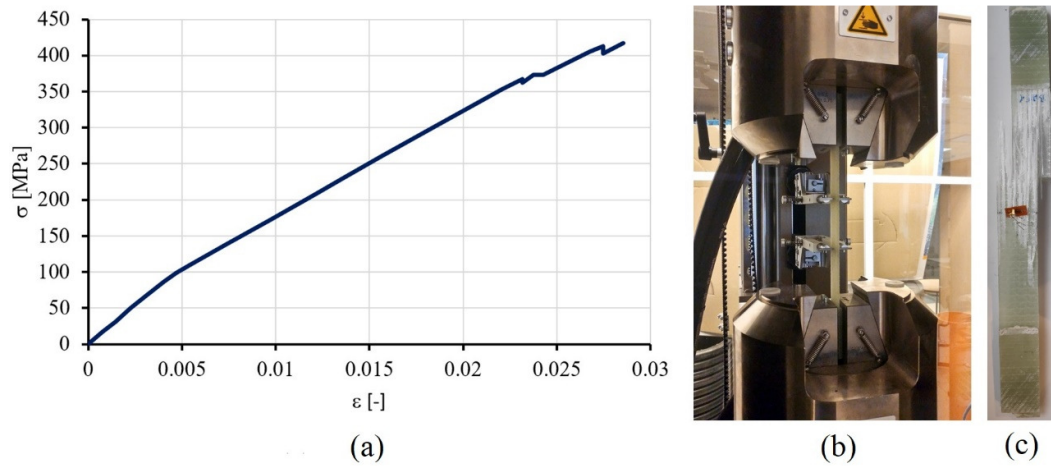
Fig. 2 Tension test of laminate coupon made of BAT [0/90] fabrics only: stress-strain relation for the laminate ply (a), test (b), specimen after failure (c)

(a)

(b)
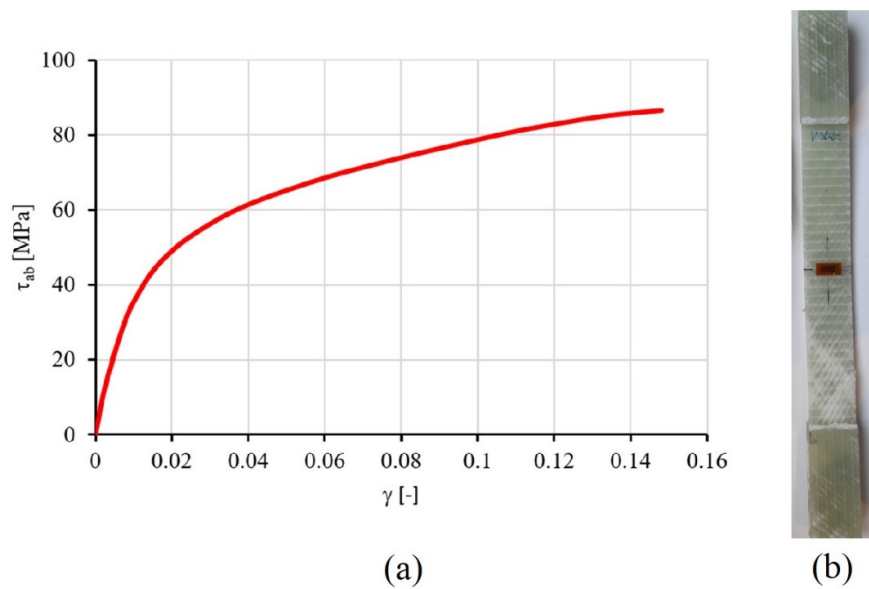
Fig. 3 Tension test of laminate coupon made of GBX [+/-45] fabrics only: stress-strain relation for the laminate ply (a); specimen after failure (b)
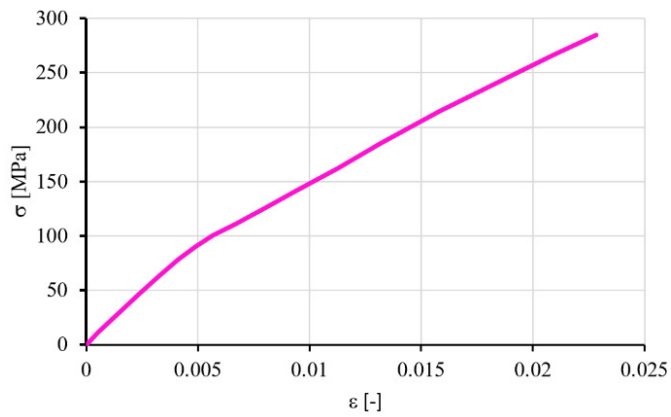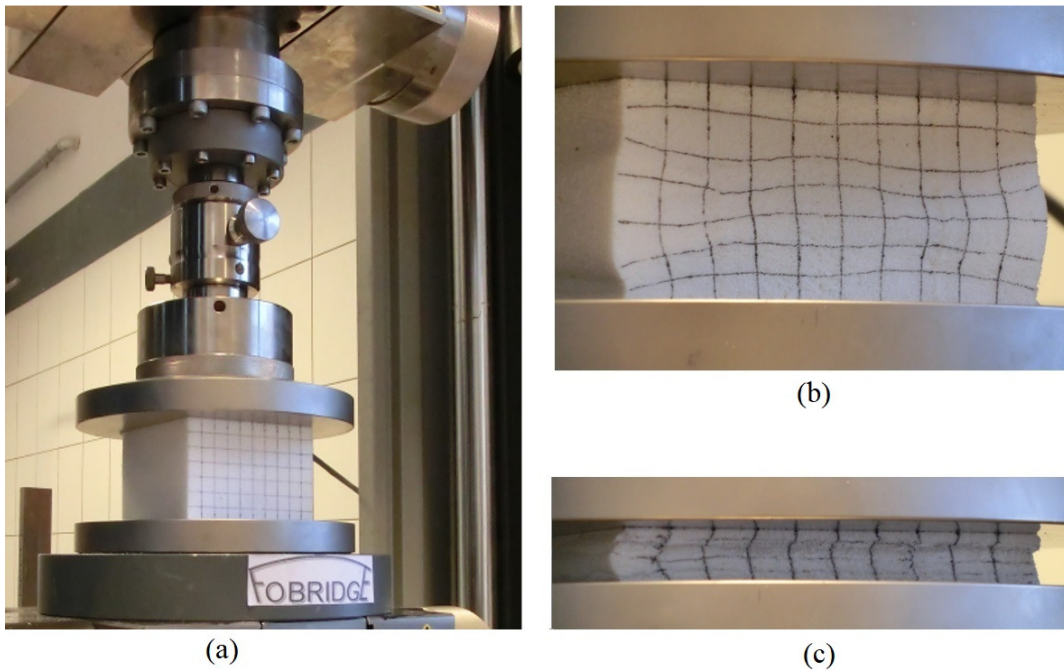
Fig. 4 Tension test of laminate coupon made of [BAT/GBX]$_s$ fabrics: stress-strain relation for the whole laminate

(b)

(a)

(c)

Fig. 5 Compression test of the AC100 foam. The specimen: at the test stand (a), during (b) and at the end (c) of the test
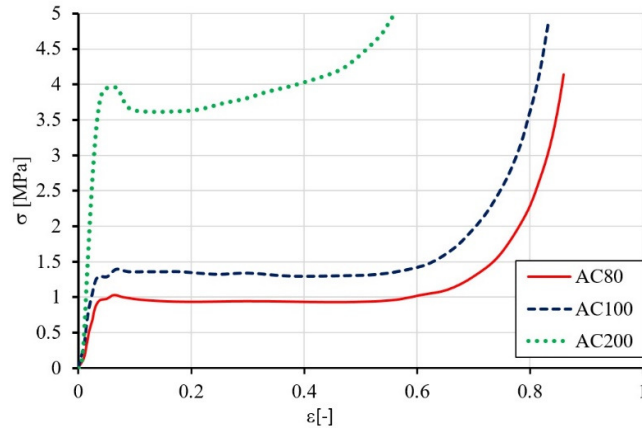
Fig. 6 Uniaxial compression tests of AC80, AC100, AC200 foams: uniaxial stress vs. strain

(a)   (b)   (c)
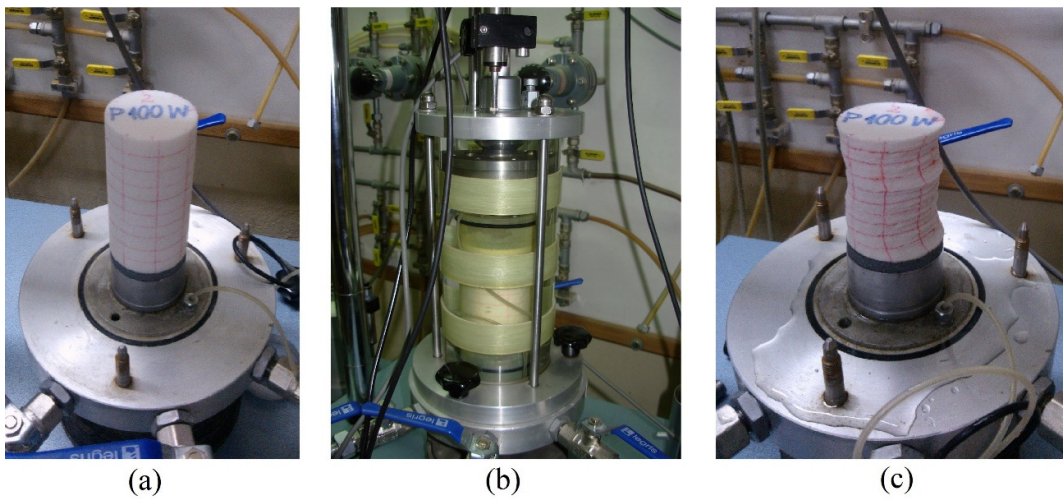
Fig. 7 Hydrostatic compression test of the AC100 foam. The specimen: before the test (a), during hydrostatic compression in the apparatus (b), after the test (c)
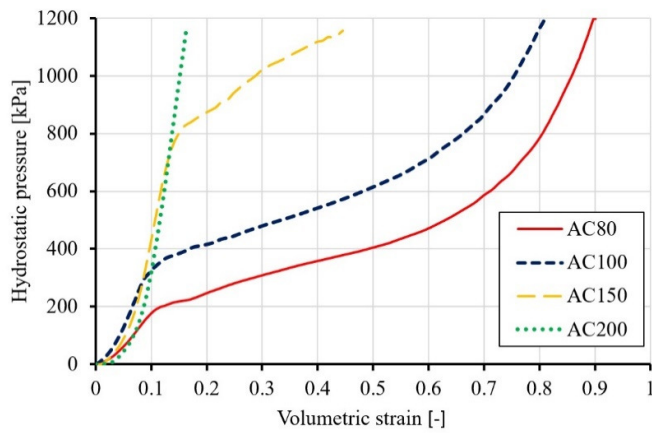
Fig. 8 Hydrostatic compression tests of AC80, AC100, AC200 foams: hydrostatic pressure vs. volumetric strain
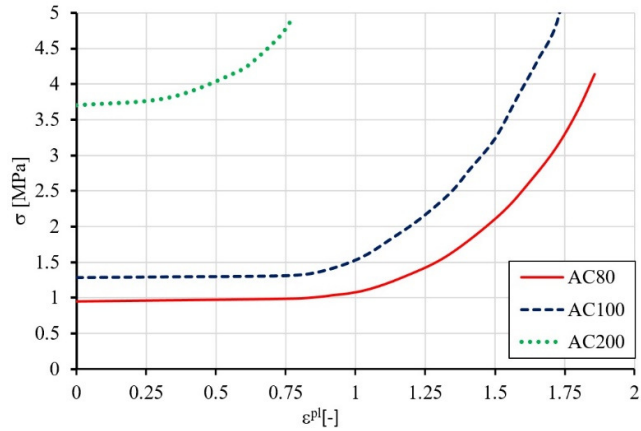
Fig. 9 Crushable foam volumetric hardening for AC80, AC100, AC200 foams: uniaxial stress vs. plastic strain
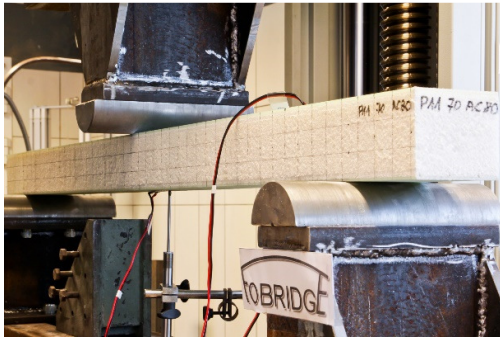
Fig. 10 The three–point bending test stand
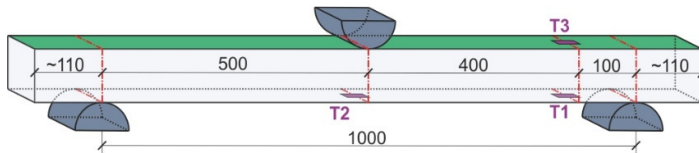
Fig. 11 Scheme of the test stand and location of strain gauges
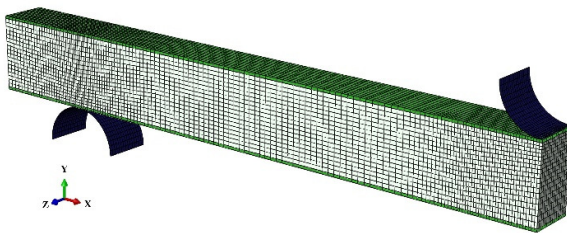
Fig. 12 Visualisation of the beam computational model: foam core – C3D8R elements (light grey); FRP face sheets – S4R elements (green, shell thickness is turned on); cross–head and steel support – R3D4 rigid elements (dark blue)
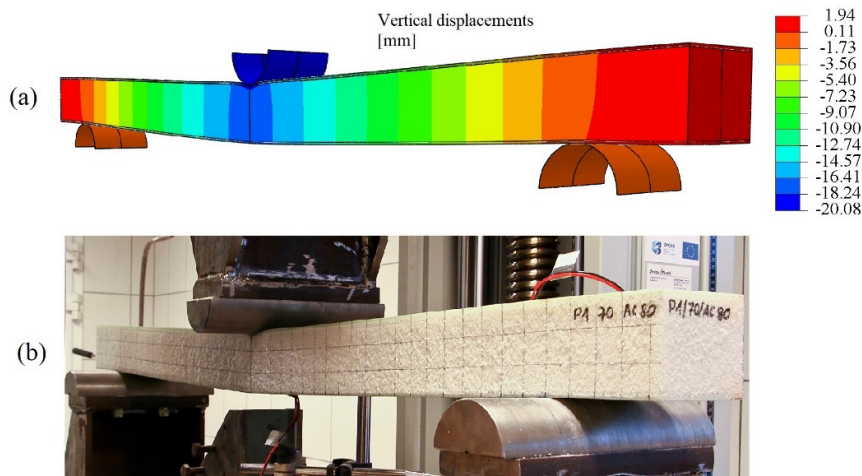
Fig. 13 Comparison of the AC80 beam deformations shortly before failure, when the cross-head displacement equals 20mm: FEM (a), experiment (b)
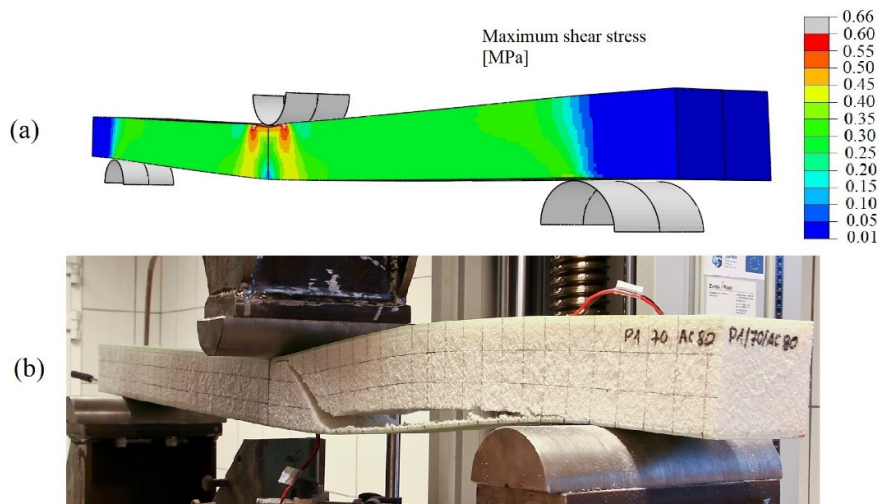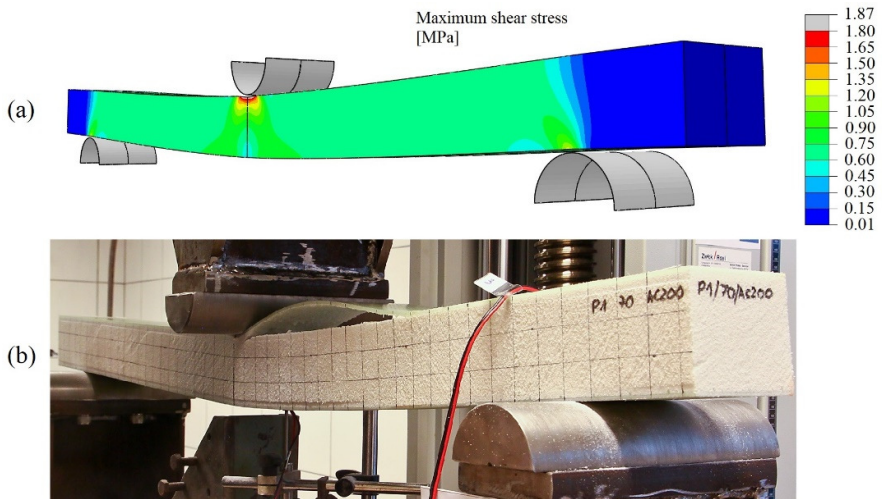

Fig. 14 The AC80 beam at the moment of failure: FEM Tresca Stress distributions (a), experiment (b)
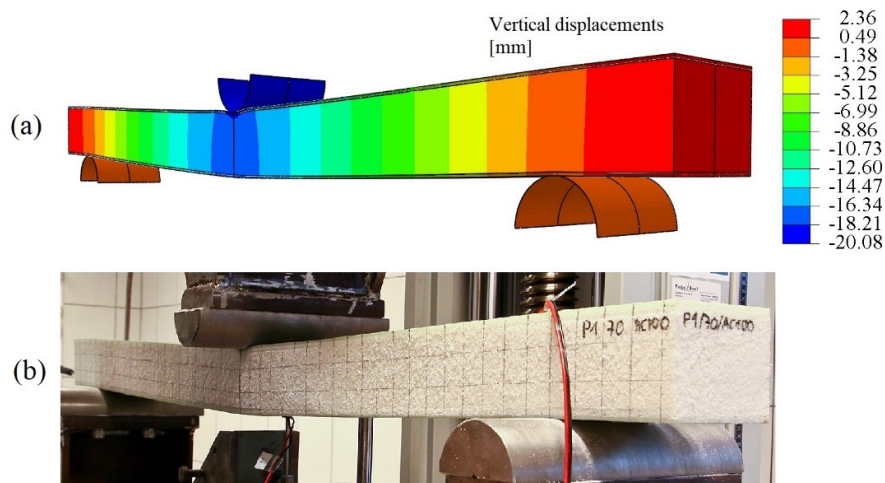
Fig. 15 Comparison of the AC100 beam deformations shortly before failure, when the cross-head displacement equals 20mm: FEM (a), experiment (b)
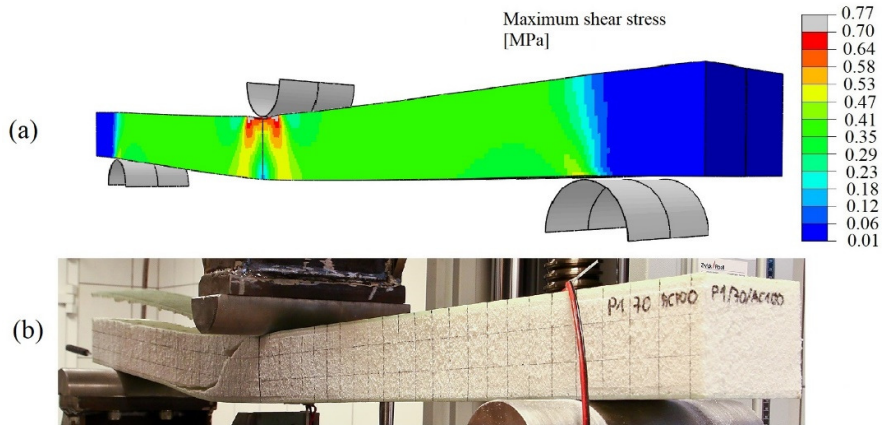
Fig. 16 The AC100 beam at the moment of failure: FEM Tresca Stress distributions (a), experiment (b)
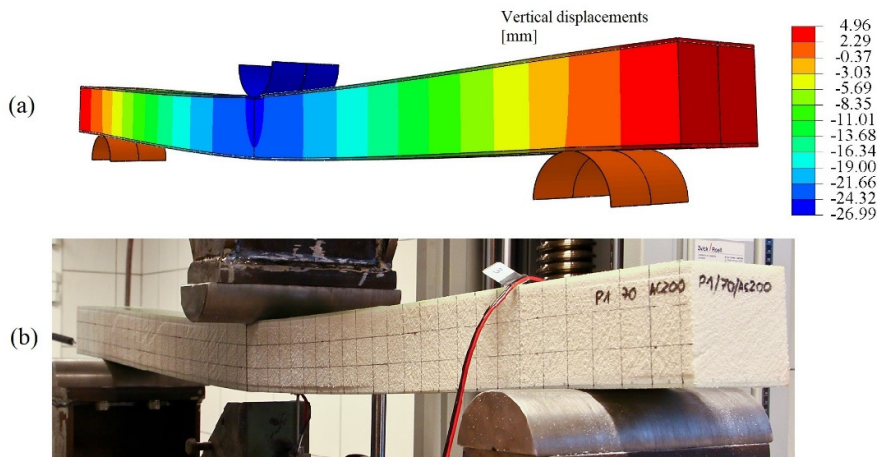
Fig. 17 Comparison of the AC200 beam deformations shortly before failure, when the cross-head displacement equals 27mm: FEM (a), experiment (b)

Fig. 18 The AC200 beam at the moment of failure: FEM Tresca Stress distributions (a), experiment (b)
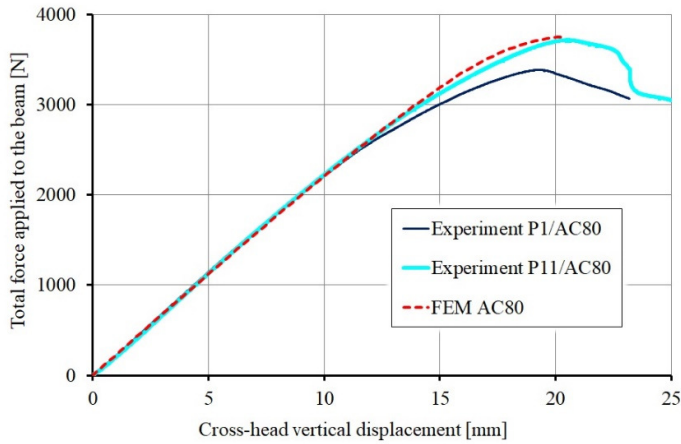
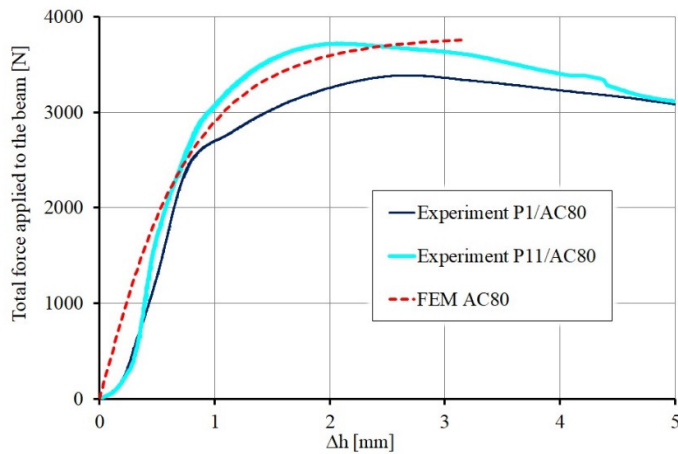Fig. 19 The relation between the total force applied to the beam and cross-head vertical displacement for the beams with AC80 core

Fig. 20 The relation between the total force applied to the beam and the reduction of core thickness Δh at the mid-span for the beams with AC80 core
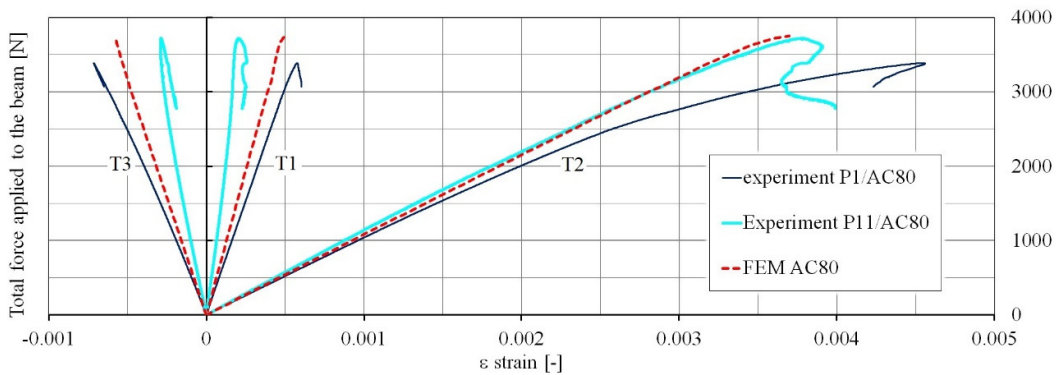

Fig. 21 Force applied to the beam vs. strain measured in T1, T2 and T3 for the beams with AC80 core
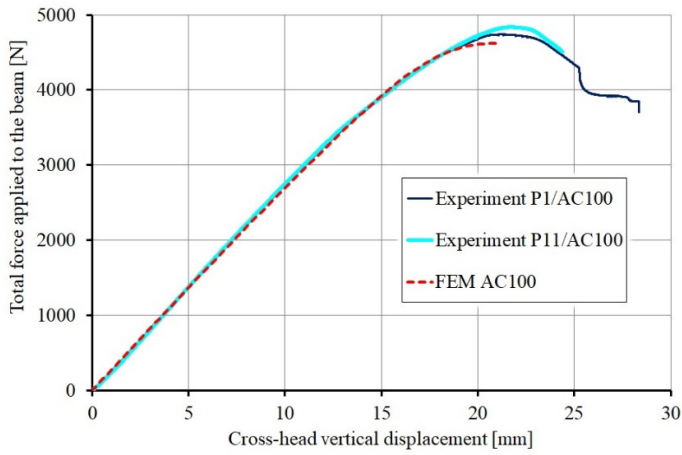
Fig. 22 The relation between the total force applied to the beam and cross-head vertical displacement for the beams with AC100 core
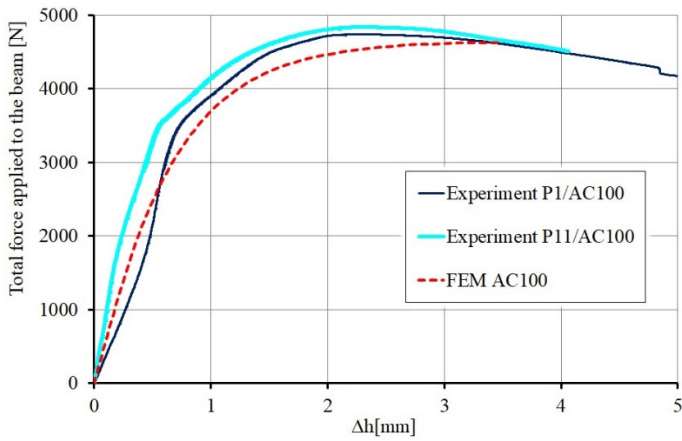

Fig. 23 The relation between the total force applied to the beam and the reduction of core thickness Δh at the mid-span for the beams with AC100 core
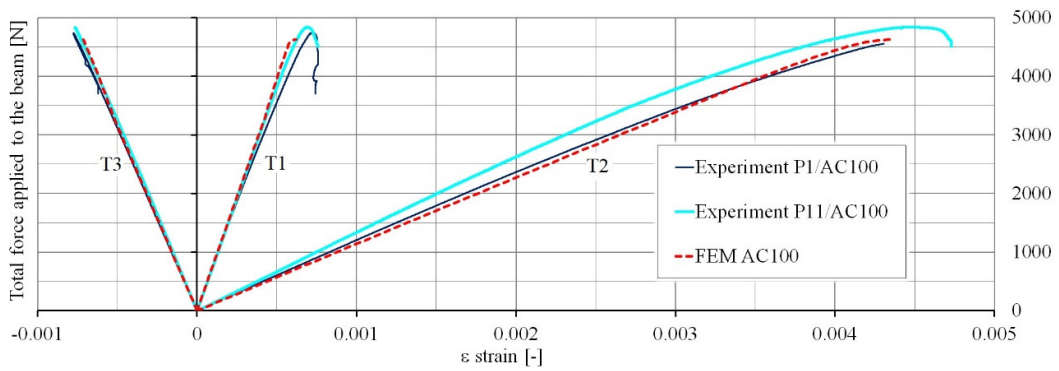

Fig. 24 Force applied to the beam vs. strain measured in T1, T2 and T3 for the beams with AC100 core
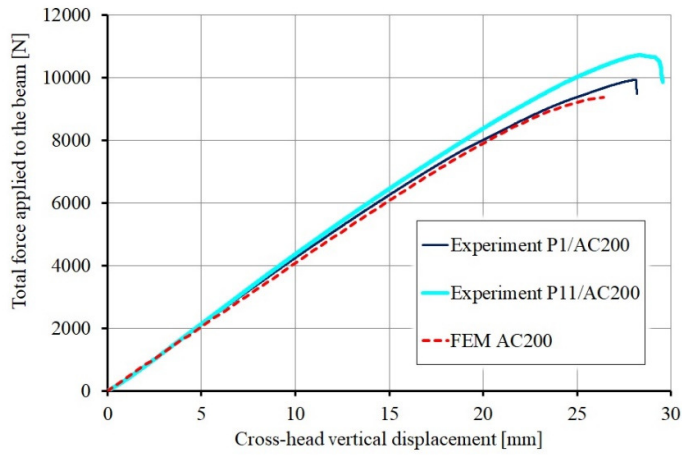
Fig. 25 The relation between the total force applied to the beam and cross-head vertical displacement for the beams with AC200 core
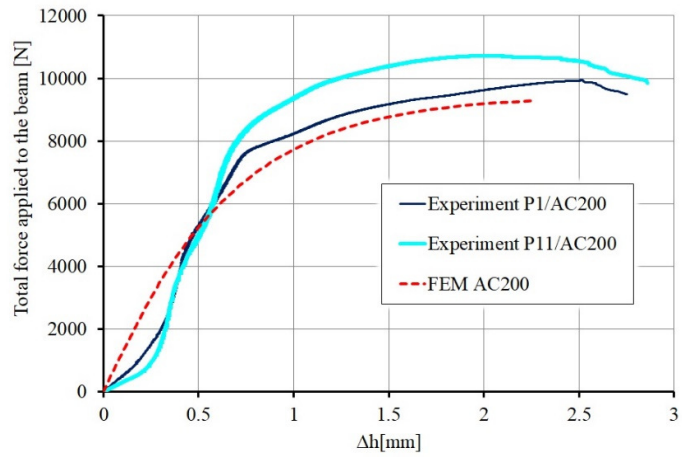

Fig. 26 The relation between the total force applied to the beam and the reduction of core thickness Δh at the mid-span for the beams with A2100 core
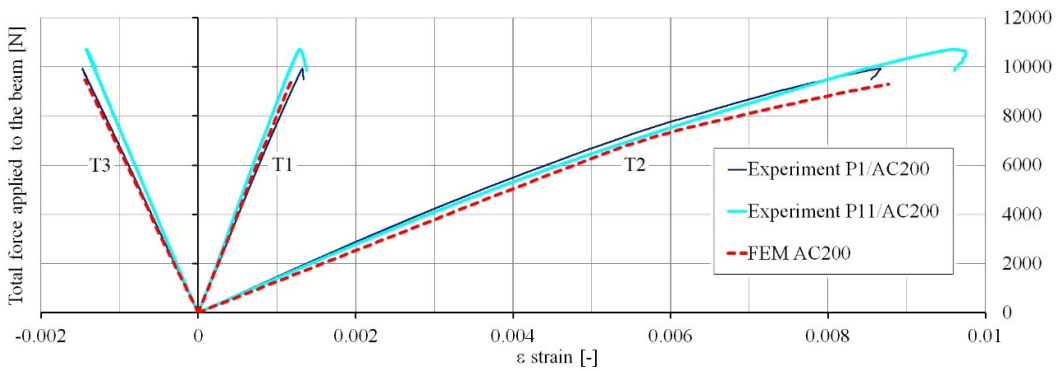

Fig. 27 Force applied to the beam vs. strain measured in T1, T2 and T3 for the beams with AC200 core
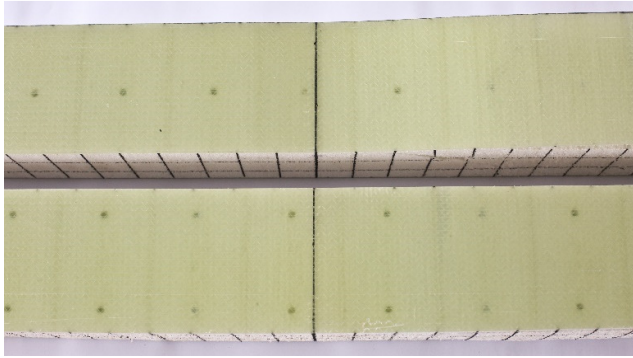
Fig. 28 Two sandwich beams seen from the top - additional resin columns are visible through the face sheet.

Tables

Tab. 1 Elastic constants of of the analysed laminate ply

	Elastic moduli [GPa]		Shear moduli [GPa]			Poisson's ratio [-]
	longitudinal	transverse	in-plane	transverse	transverse	in-plane
	E_1	E_2	G_{12}	G_{13}	G_{23}	v_{12}
	23.4	23.4	3.52	1.53	1.53	0.153

Tab. 2 Elastic constants and strengths of the ArmaForm PET/W AC ([58])

Foam	Elastic moduli [MPa]		Shear modulus [GPa]		Strengths [MPa]		
	tensile	compression		tensile	compression	shear	
	E_t	E_c	G	f_t	f_c	f_s	
AC80	75	60	15	2.1	0.95	0.6	
AC100	105	70	20	2.4	1.50	0.85	
AC200	230	157	50	4.4	3.60	1.8	

Tab. 3 Elastic constants and strengths determined in experiments for AC80, AC100 and AC200 foams

Foam	Elastic modulus [MPa]	Strengths [MPa]	
		uniaxial compression	hydrostatic compression
	E	f_c	f_c^h
AC80	40	1.02	0.20
AC100	57	1.26	0.38
AC200	148	3.99	1.6

Tab. 4 Comparison of shear modulus taken from technical data sheet and the present one derived from uniaxial compression test in the core thickness direction and for $v=0.4$

Foam	Shear modulus [MPa]		Relative difference [%]
	Technical data sheet	Actual	
AC80	15.0	14.3	4.7
AC100	20.0	20.3	1.5
AC200	50.0	52.9	5.8

Tab. 5 Parameters of isotropic crushable foam plasticity model for ArmaForm PET/W AC80, AC100 and AC200

Foam	AC80	AC100	AC200
Elastic modulus [MPa]	40	57	148
Poisson's ratio	0.4	0.4	0.4
Compression yield stress ratio	2.99	2.99	2.49
Hydrostatic yield stress ratio	1.0	1.0	1.0
Crushable foam hardening	Fig. 9	Fig. 9	Fig. 9

Tab. 6 Comparison of sandwich beams failure loads

Foam	FEM estimation [N]	experimental failure load [N]			Relative difference [%]
		P1	P11	P^{avg}	
AC80	3700	3385	3750	3568	3.7
AC100	4610	4740	4800	4770	3.4
AC200	9280	10000	10700	10350	10.3